ARTICLE

Check for updates

Fractional correlated insulating states at one-third filled magic angle twisted bilayer graphene

Kevin Zhang [1]✉, Yang Zhang [2], Liang Fu [2] & Eun-Ah Kim[1]

The observation of superconductivity and correlated insulating states in twisted bilayer graphene has motivated much theoretical progress at integer fillings. However, little attention has been given to fractional fillings. Here we show that the three-peak structure of Wannier orbitals, dictated by the symmetry and topology of flat bands, facilitates the emergence of a state we name a "fractional correlated insulator" at commensurate fractional filling of $\nu = n \pm 1/3$. Specifically for the filling of 1/3 electrons per moiré unit cell, we show that short-range interactions lead to an extensive entropy due to the "breathing" degree of freedom of an irregular honeycomb lattice that emerges through defect lines. The leading further-range interaction lifts this degeneracy and selects a ferromagnetic nematic state that breaks AB/BA sublattice symmetry. The proposed fractional correlated insulating state might underlie the suppression of superconductivity at $\nu = 2 - 1/3$ filling observed in ref. [1].

[1] Laboratory of Atomic and Solid State Physics, Cornell University, 142 Sciences Drive, Ithaca, NY 14853-2501, USA. [2] Condensed Matter Theory Group, Massachusetts Institute of Technology, 77 Massachusetts Avenue, Cambridge, MA 02139, USA. ✉email: kz345@cornell.edu

apid developments in twisted bilayer graphene (TBG) so far have mostly focused on integer fillings, starting with the initial discovery of correlated insulating states at an integer number of electrons per moiré unit cell[2]. There has been much progress driven by experimental discoveries of orbital ferromagnetism[3–5] and other isospin polarization[6] as well as nematic tendencies[1,7,8]. However, less attention has been given to studies of fractional filling, although phase diagrams have shown potentially nontrivial phenomena at partial fillings, such as suppression of superconductivity near the filling of $\nu = 2 - 1/3$[1].

The focus on integer filling from a theoretical standpoint comes from the complexity of the microscopic description of magic angle TBG (MATBG). While experimentally, MATBG exhibits itself as a triangular superlattice[4,8–10], it has been shown that local Wannier orbitals centered at triangular lattice sites are obstructed due to the symmetry and topology of the Bloch wavefunctions[11–14]. Instead, maximally localized Wannier orbitals are centered at AB or BA sites with three lobes of the wavefunction extending to the three neighboring AA sites[15–17] (Fig. 1). Such extended Wannier orbitals are challenging for attempts to formulate a local model, necessarily introducing further-range hopping and interaction terms[15,16]. Little attention has been given to the fact that at commensurate partial fillings of $n \pm 1/3$ (with n integer), strong short-range interactions give rise to geometric constraints. However, historically, interaction-driven phenomena at partial fillings have been full of surprises and new physics, and hetero-transition metal dichalcogenide moiré systems have shown previously unseen charge-ordered states[18–20]. Furthermore, geometrically constrained systems have long been fertile grounds for new emergent phenomena as evidenced by the rich physics of spin ice[21] and spin liquids[22].

In this article, we focus on the implications of the Wannier obstruction and the extended Wannier orbitals in MATBG at the partial commensurate filling of $\nu = 1/3$ electrons per unit cell. Focusing on the strong-coupling limit invites us to map our problem onto that of a tiling problem[23,24]. Through this mapping, we argue for an extensive degeneracy of ground states at $\nu = 1/3$, filling in the limit of short-range interactions. We then discuss how that degeneracy is lifted by the direct ferromagnetic exchange when further-range interactions[16] are taken into

account. The exchange interaction selects a nematic state with ferromagnetic spin order. Nevertheless, the extensive degeneracy in the strong-coupling limit would still be visible as an enhancement in entropy at temperatures exceeding the energy scale of ferromagnetic exchange. We then confirm this prediction based on energetics through Monte Carlo simulations.

Results and discussion

Model. We start with the much-studied lattice model of MATBG[15,16]. The offset angle between the two stacked hexagonal lattices of MATBG leads to a long-period moiré pattern that forms the relevant lattice (Fig. 1a). Within the moiré pattern, one can identify "AA" sites where the two layers are maximally aligned, along with "AB" or "BA" sites where the two layers are maximally offset. At the particular twist angle known as the "magic" angle, the low-energy bands are flat and isolated, allowing us to focus on the interactions of low-energy Wannier orbitals. The Wannier orbitals of this system have a peculiar extended "fidget spinner" shape, as was found in ref. [16]. This can be understood through symmetry considerations: while the predicted[25,26] and observed[9,27,28] local density of states (LDOS) of MATBG are peaked at AA sites corresponding to a triangular lattice, any prescription of orbitals localized to these same triangular lattice sites cannot reproduce the required band structures at the high symmetry points of the moiré Brillouin zone[11,13]. In fact, the only option is for the orbitals to be located at AB and BA sites, forming a honeycomb lattice, in direct analogy with monolayer graphene. Thus, the charge density of a maximally localized WS (Wannier state) must be split among the centers of the three neighboring plaquettes (red and blue blobs in Fig. 1a). Although additional bands beyond the flat bands are required for the WSs to capture all the symmetries of free-standing TBG due to the Wannier obstruction[17,29], hBN-aligned samples or disordered samples may break C_2T or other symmetries. For simplicity, we restrict our analysis to the WSs of the flat bands, which always have the same three-lobed shapes regardless of the explicit construction[11,15,16]. As a natural consequence of the WS being extended, the range of on-site interactions of fractional charges is longer than usual. However, little attention has been given to the implications of these "distant" interactions at fractional filling factors.

Immediately, one can recognize that the largest on-site repulsion will arise when two Wannier orbitals have an overlapping lobe (Fig. 1a). This was confirmed by a direct construction of maximally localized WSs[16]. At small filling factors, the ground-state configuration must therefore have no overlap between triangles. Interestingly, at the particular filling of $\nu = 1/3$ (one WS for every three AA sites), configurations exist in which each AA site hosts a 1/3 charge lobe while the WSs respect the no-touching rule. These configurations would all be incompressable and thus suggest the existence of a fractional correlated insulating state. To better illustrate these no-touching configurations, we introduce the graphical notation of representing WSs as triangles. Their three-pronged "fidget spinner" shape can be equivalently represented by a triangle (Fig. 1b), where the vertices of the triangle correspond to charge lobes of the WS. In other words, the no-touching rule of the WSs is equivalent to enforcing that no two triangles share a vertex. For example, the gray triangles in Fig. 1b would all violate the no-touching rule with respect to the central triangle. Then, our triangle representation of the WSs combined with the hard "no-touching" constraint allows us to map MATBG at $\nu = 1/3$ to a lattice tiling problem.

Specifically, we draw a parallel to the triangular trimer tiling model of ref. [24], in which trimers are placed on a triangular lattice
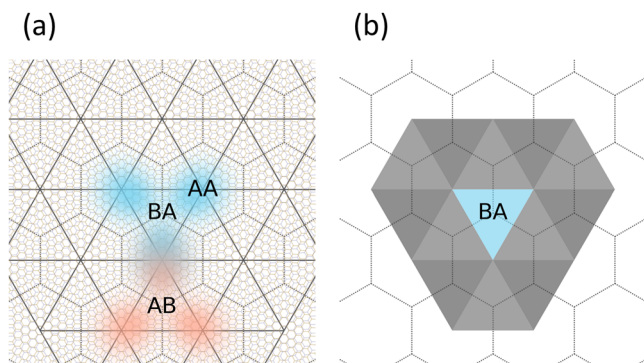

Fig. 1 Visualization of Wannier states (WSs), AA, and AB/BA sites in twisted bilayer graphene. a An example of a typical moiré pattern formed by a system with a twist angle of 6°. The moiré unit cells are delimited by the honeycomb lattice, and its dual triangular lattice is also shown. The blue and red blobs schematically represent the shape of Wannier orbitals on the BA and AB sublattices, respectively, with one overlapping charge lobe. **b** Schematic representation of the central WS in (**a**) as a blue triangle, where the vertices of the triangle correspond to the three charge lobes. The gray triangles show those WSs which have at least one lobe overlapping with the central blue WS; in other words, they share vertices with the central triangle.
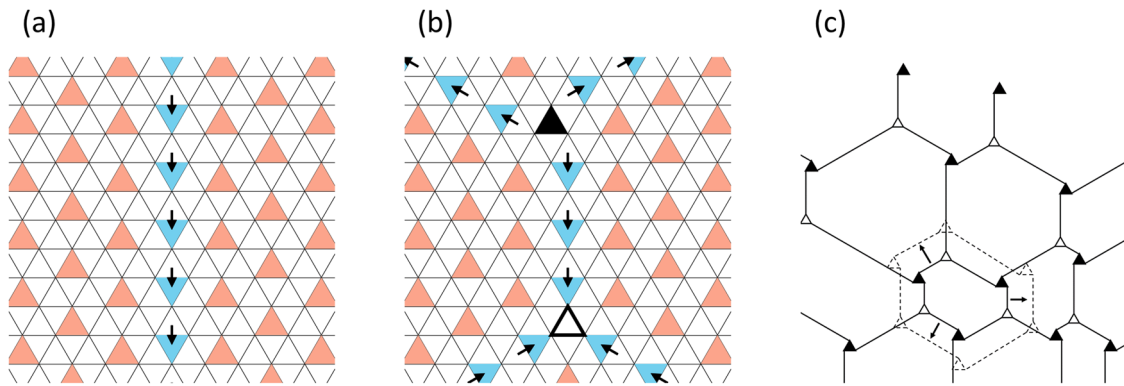
Fig. 2 Visual representation of the "breathing entropy" argument for no-touching trimer tilings. a Starting from a uniform and sublattice-polarized $\sqrt{3} \times \sqrt{3}$ state (red triangles), a line of trimers can be "flipped" (from red to blue triangles), which spans the length of the sample. Any such line of flips must span the sample, and there are three directions a line can extend in. **b** Three lines of flips can either meet in an inverted "Y" joint (bottom), resulting in a vacancy of the original $\sqrt{3} \times \sqrt{3}$ configuration (open black triangle), or in an upright "Y" joint (top), resulting in the addition of a new Wannier state (filled black triangle). **c** Together, the three line directions and two types of junctions form a network of irregular hexagons. As the locations of the joints are not fixed, the hexagons can be freely deformed (black arrows), leading to the extensive "breathing entropy" of the system.

such that no two trimers overlap. Within this model, a fully flavor polarized state occupying 1/3 of all AB sites and maintaining C_3 symmetry is a ground state. This state is represented by a complete tiling of AB triangles, which we name the "$\sqrt{3} \times \sqrt{3}$" state. Starting from this isotropic state, an isolated flip of an AB (red) triangle to a neighboring BA (blue) triangle takes the system outside of the ground-state manifold, as one vertex of the flipped triangle will inevitably touch a neighboring triangle. However, the no-touching constraint can be maintained if the flipping is continued along a line perpendicular to the flipping axis (Fig. 2a). The freedom in the flipping hints that the ground-state manifold could contain a macroscopic number of zero-energy states. In fact, the trimer tiling problem was found to have extensive ground-state entropy[24], despite the prohibition of any local moves for individual triangles.

Ground states and lifting degeneracy. While the exact solution of the trimer tiling problem in ref. [24] makes use of the Bethe ansatz to explicitly calculate the extensive entropy (see Supplementary Note I for details), the extensivity of the ground-state entropy can also be understood through purely geometric considerations. We briefly summarize the geometric argument of Verberkmoes and Nienhuis[24] below. Starting from lines of flipped triangles mentioned above, which we dub "flip-lines", we observe that there are three directions that the flip-lines can extend along, each perpendicular to the three sides of an AB triangle. The flip-lines can only terminate at one of two types of Y-junctions (see Fig. 2b): one that introduces a vacancy (empty black triangle) or one that adds a WS (filled black triangle). Further, each flip-line segment must pair an empty junction and a full junction, which effectively transports charge along the segment while staying within the ground-state manifold without changing the net filling. Since each segment terminates at Y-junctions, these segments form an irregular honeycomb network in the limit of dilute flip-lines. The irregularity of the network gives individual hexagons the freedom to expand or shrink (Fig. 2c) at no energy cost, which drives the extensive entropy of the system. The mechanism for the entropy under the "no-touching" constraint is analogous to the mechanism for the "breathing entropy" in krypton adsorbed on graphite[30,31] where domain walls were predicted to also form an irregular honeycomb network.

Now, we turn to further-range interactions that break the degeneracy. Notably, our "no-touching" model restricted to local interactions has zero Hamiltonian since the flip-lines and the

Y-junctions cost no energy, unlike in the case of krypton adsorbed on graphite[30,31]. Since the degeneracy consists of states that all have the same uniform charge density but the differing layout of WSs, a long-range density-density Coulomb interaction would not break the degeneracy. Further, as we show in Supplementary Note II, the interaction terms proposed in ref. [32] would not change the ground-state manifold. Therefore, the leading further-range perturbation is direct exchange between fourth-nearest neighbor WSs on opposite sublattices, labeled as the J_4 interaction in ref. [16] (Fig. 3a, c; see Supplementary Note III for a discussion of further range interactions). This interaction couples pairs of WSs on opposite sublattices ferromagnetically. Hence, the J_4 interaction breaks sublattice degeneracy as well as spin degeneracy. Moreover, J_4 couples only WSs in the same valley, meaning that the resultant state would be valley polarized. From the perspective of the flip-line picture, the J_4 interaction promotes flip-lines by introducing *negative* energy per unit length of flip-lines. This is unusual from the perspective of the domain wall network[30,31], suggesting that a different approach may be needed to analyze the situation.

We can readily understand the ground states selected by the J_4 interaction by inspecting the number of J_4 bonds each WS can have. As shown in Fig. 3a, c, each WS has six neighboring sites it can couple to though the J_4 interaction. Although the energy gain of the J_4 interaction would promote flipping as many triangles as possible, starting from the bulk $\sqrt{3} \times \sqrt{3}$ state, at most only three of the six neighbors can be occupied while respecting the no-touching constraint. A tiling pattern that saturates this limit has to be a type of hexagonal lattice. Given the underlying structure and the no-touching constraint, the hexagonal tiles need to be anisotropic and slanted. Further details of this construction can be found in Supplementary Note III. From this, one can build patterns with three J_4 bonds per WS by tiling slanted and elongated hexagonal bricks, with two possible directions for slanting in a given row (Fig. 3b, d). Since the bricks are elongated, the arrangement of the WSs breaks rotational symmetry, resulting in a nematic charge order with ferromagnetic spin order that also breaks sublattice symmetry and mirror symmetry. At the same time, the residual degeneracy due to the slanting degree of freedom for each row may further be broken with longer range interactions. While the energy difference of the J_4 splitting is on the order of 0.1 meV[16], the kinetic energy of the extended Hubbard model of Kang and Vafek[15] would favor the $\sqrt{3} \times \sqrt{3}$ state with an extremely small energy difference on the order of 10^{-6} meV; see Supplementary Note IV.
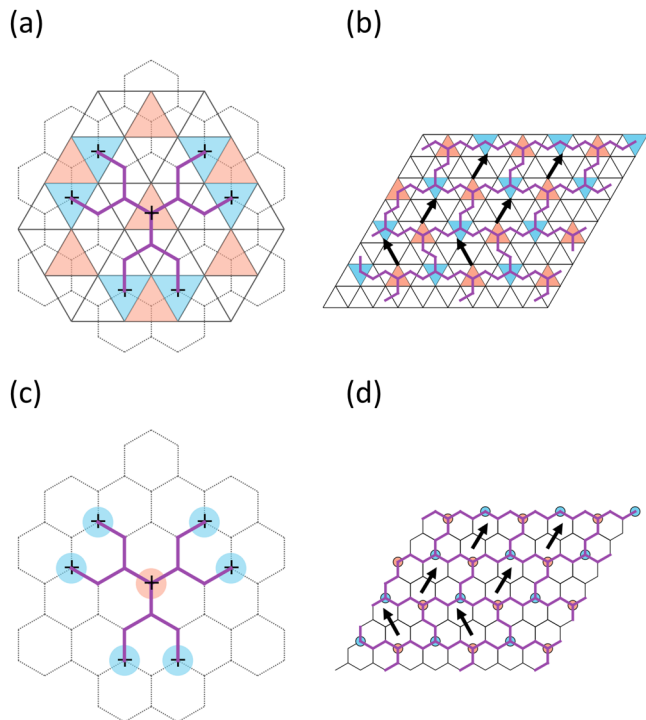
Fig. 3 Visualization of the J_4 interaction range, and the J_4-optimal state in two representations. The red and blue colorings correspond to Wannier states (WSs) on the AB and BA sublattices, respectively. **a** The red triangles represent a $\sqrt{3} \times \sqrt{3}$ state. With respect to the central red triangle, there are six possible J_4 neighbors, shown by the blue triangles. Only three of the six J_4 locations can be simultaneously occupied. **b** A configuration with the maximum number of three J_4 neighbors per state, and thus the lowest possible energy. The purple line segments mark pairs of states that are coupled by the J_4 interaction. The lines of J_4 couplings form an anisotropic emergent hexagonal, or "brick", lattice. The nematicity arises from the rotational symmetry breaking in the spatial arrangement of the WSs. **c**, **d** Same as panels **a** and **b**, but in the WS center site representation.

Monte Carlo. Monte Carlo simulations provided further insight. Using finite temperature Metropolis–Hastings Monte Carlo simulation, we identified numerous ground states at low temperature in the no-touching model, agreeing with the predicted extensive degeneracy. Then, we studied degeneracy lifting by adding in J_4 direct exchange as a perturbation, which resulted in the selection of a unique stripe charge-ordered state (Fig. 4a). This state has the same form as that predicted in Fig. 3b, d, but does not show row-wise freedom in the "brick" slant orientations. Because changing the orientation of an entire row of bricks would require a simultaneous semi-global update of a row, freedom in the brick orientations would only be rarely observed in the simulations that we have performed. Still, these results support our predictions for the no-touching model, and additionally provided numerically evaluated estimates for the entropy (see "Methods" for details).

Summary. To summarize, we have proposed a mechanism for translationally symmetric fractional correlated insulating states in MATBG. The incompressibility of the $n \pm 1/3$ states is a robust consequence of the Wannier obstruction in MATBG. With the Wannier orbitals' weight split into three lobes, the shortest interaction promotes a uniform distribution of charge, where a third of charge is centered at each AA site. This gives rise to charge order at fractional filling. Mapping the model to that of a trimer tiling problem, we showed that the short-range no-
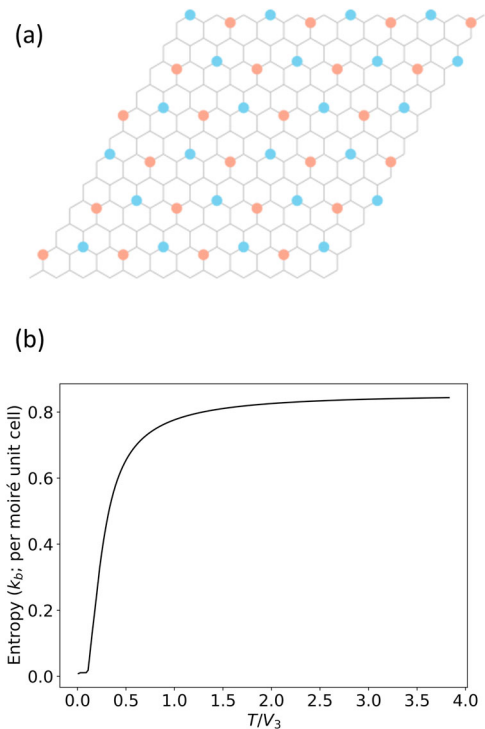
Fig. 4 Monte Carlo simulation results. a A ground state of the "no-touching" plus J_4 model, found through Monte Carlo with periodic boundary conditions. This state is equivalent to that predicted in Fig. 3b, d, but does not display freedom in the bricks' slant directions. **b** Entropy of the "no-touching" model, with J_4 perturbation, as a function of temperature, neglecting spin and valley degrees of freedom. The temperature is reported in units of V_3, which represents the strength of the repulsive Coulomb interaction for third-nearest neighbor Wannier states (see Supplementary Note III for the definition of V_3).

touching limit alone would imply an extensive entropy. The dominant further-range interaction amounts to direct exchange, which favors the ferromagnetic order. The direct exchange lifts the degeneracy and selects a highly nontrivial state which breaks C_3 rotational symmetry, AB/BA sublattice symmetry. Further, it has an antiferromagnetic arrangement of AB/BA Wannier centers, while being spin ferromagnetic. In this state, the multiple sectors of spin, orbital, and spatial rotation are intertwined. In arriving at our conclusions about degeneracy splitting in this work, we have focused on exchange interactions, as well as hopping as a perturbation. More broadly, quantum fluctuations would split the degeneracy, and order-by-disorder would also likely pick a ground state, which could be a subject of future study.

Discussion. Although no experiments have targeted the fractional correlated insulating state that we proposed yet, recent experiments show compelling support for our predictions. First, Cao et al.[1] found a dip in the superconducting T_c at $v = 2 - 1/3$, which is reminiscent of the dip in T_c in high-T_c cuprates at a commensurate filling of 1/8 holes per copper oxide plane[33]. Furthermore, at this filling, upon suppressing superconductivity with a magnetic field, the system stayed insulating down to the lowest temperatures studied. Moreover, in zero field, anisotropic magnetotransport was observed. This suggests a correlated insulating state competing with superconductivity at this filling. While in cuprates, this so-called 1/8 anomaly is associated with translational symmetry breaking charge-ordered (stripe) states, the extended Wannier orbitals and topological obstruction in TBG
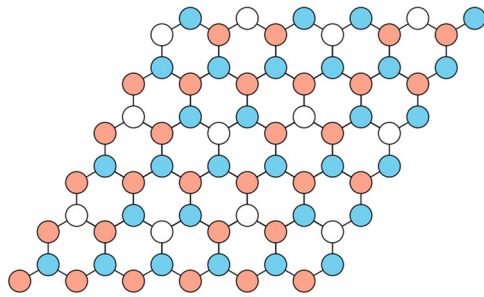
Fig. 5 One example of a nematic charge-ordered state at $\nu = 2 - 1/3$ filling. The configuration was obtained by subtracting the $\nu = 1/3$ state (i.e., that shown in Fig. 3b, d) from a uniform $\nu = 2$ state proposed in refs. [15,16]. The filled red and blue circles represent filled Wannier states on the AB and BA sublattices, respectively, while empty circles represent holes relative to the uniform $\nu = 2$ state. Since the holes are placed in the same pattern as Fig. 3b, d, the resulting $\nu = 2 - 1/3$ state is also nematic. Similarly, this state is also ferromagnetic due to the exchange interactions between the Wannier states.

imply a very different type of charge-ordered state whose Wannier centers break lattice translational symmetry but the charge distribution itself respects lattice translational symmetry. This is a unique possibility afforded by the topological obstruction in MATBG. Rozen et al.[34] found entropy to slowly decrease with decreasing temperature at higher temperatures until it drops with ordering at lower temperatures. This closely resembles how the extensive entropy of the short-range interacting model was visible to the system at temperature scales higher than the interactions in our simulation. Although a careful study of how to extend our prediction to general states $\nu = n \pm 1/3$ would be an interesting future direction, we present here a candidate state for $\nu = 2 - 1/3$ to match the experimentally observed phenomena. To construct $\nu = 2 - 1/3$ filling states, we now take the Wannier states in Fig. 3 to be holes in a previously proposed $\nu = 2$ state[16,32]; the resultant pattern is shown in Fig. 5, and has the same nematicity, incompressibility, and ferromagneticity of our proposed $\nu = 1/3$ state. This interpretation would rule out some of the $\nu = 2$ states in ref. [16] that cannot support the hole pattern of Fig. 3. In addition to experimental tests of our predictions, the effects of quantum fluctuations on our geometric perspectives promise to be a rich area of future theoretical studies as has been the case for spin ice[22].

Post completion of our work, Xie et al.[35] observed an incompressible state with Chern number 0 at $\nu = 4 + 11/3$ electrons per moiré unit cell, presenting a possible manifestation of our predicted fractional correlated insulator state. Motivated by the experiment, a Hartree–Fock calculation with a tripled superlattice in ref. [36] considered a charge-ordered state corresponding to the $\sqrt{3} \times \sqrt{3}$ tiling. The fractional correlated insulating states that we are proposing differ from the proposed Hartree–Fock states in that our states preserve translational symmetry in the charge sector, as well as hosting quasiparticles with fractional charge[37].

Methods
To simulate the extensively degenerate ground-state manifold, we performed a finite temperature Metropolis–Hastings Monte Carlo (MC) simulation of the no-touching model. We modeled the on-site interactions using the approximation of ref. [16], where WSs are approximated by three 1/3 fractional charges centered at their lobes. We then study the lifting of degeneracy by adding a small J_4 perturbation. To avoid being trapped in local minima, a single MC step consisted of independent add and remove operations, ensuring global updates. In the original no-touching model, we identified abundant ground-state charge orders at low temperature. Meanwhile, after adding the J_4 perturbation, the one-dimensional type charge order appeared to have a unique ground state as shown in Fig. 4a.

To evaluate the ground-state degeneracy, the zero-temperature thermal entropy of twisted bilayer graphene at $n = \pm 1/3$ is calculated within the no-touching model. Direct calculation requires counting in the ground-state manifold with exponentially large degeneracy, which is only possible for small-size systems. In extended systems, we first derive the infinite temperature entropy exactly and then approach the zero-temperature entropy by temperature-dependent Monte Carlo simulations. In a spin-valley fully polarized system, the exact infinite temperature entropy per moiré unit cell in the thermodynamic limit ($N \sim \infty$) is given by $S_\infty = k_B \ln Z/N^2 \approx (2 \ln 2 - n \ln n - (2 - n) \ln(2 - n)) k_B$ where Z is the dimension of the configuration space, and n is the number of charges per moiré unit cell. The temperature-dependent entropy is given by $S(T) = S_\infty - \int_T^\infty dT' C_V(T')/T'$, and $C_V(T) = \frac{\partial \langle E \rangle}{\partial T} = \frac{1}{k_B T^2}(\langle E^2 \rangle - \langle E \rangle^2)$ is the specific heat that can be directly evaluated from the energy distribution in Monte Carlo simulations (Fig. 4b).

Data availability
Data sharing is not applicable to this article, as no datasets were generated or analyzed during the current study.

Code availability
Monte Carlo code is available upon request to the authors.

References
1. Cao, Y. et al. Nematicity and competing orders in superconducting magic-angle graphene. *Science* **372**, 264–271 (2021).
2. Cao, Y. et al. Correlated insulator behaviour at half-filling in magic-angle graphene superlattices. *Nature* **556**, 80–84 (2018).
3. Sharpe, A. L. et al. Emergent ferromagnetism near three-quarters filling in twisted bilayer graphene. *Science* **365**, 605–608 (2019).
4. Choi, Y. et al. Correlation-driven topological phases in magic-angle twisted bilayer graphene. *Nature* **589**, 536–541 (2021).
5. Wu, S., Zhang, Z., Watanabe, K., Taniguchi, T. & Andrei, E. Y. Chern insulators, van hove singularities and topological flat bands in magic-angle twisted bilayer graphene. *Nat. Mater.* **20**, 488–494 (2021).
6. Saito, Y. et al. Isospin Pomeranchuk effect in twisted bilayer graphene. *Nature* **592**, 220–224 (2021).
7. Jiang, Y. et al. Charge order and broken rotational symmetry in magic-angle twisted bilayer graphene. *Nature* **573**, 91–95 (2019).
8. Kerelsky, A. et al. Maximized electron interactions at the magic angle in twisted bilayer graphene. *Nature* **572**, 95–100 (2019).
9. Luican, A. et al. Single-layer behavior and its breakdown in twisted graphene layers. *Phys. Rev. Lett.* **106**, 126802 (2011).
10. Xie, Y. et al. Spectroscopic signatures of many-body correlations in magic-angle twisted bilayer graphene. *Nature* **572**, 101–105 (2019).
11. Po, H. C., Zou, L., Vishwanath, A. & Senthil, T. Origin of mott insulating behavior and superconductivity in twisted bilayer graphene. *Phys. Rev. X* **8**, 031089 (2018).
12. Song, Z. et al. All magic angles in twisted bilayer graphene are topological. *Phys. Rev. Lett.* **123**, 036401 (2019).
13. Yuan, N. F. Q. & Fu, L. Model for the metal-insulator transition in graphene superlattices and beyond. *Phys. Rev. B* **98**, 045103 (2018).
14. Song, Z.-D., Lian, B., Regnault, N. & Bernevig, B. A. Twisted bilayer graphene. ii. stable symmetry anomaly. *Phys. Rev. B* **103**, 205412 (2021).
15. Kang, J. & Vafek, O. Symmetry, maximally localized Wannier states, and a low-energy model for twisted bilayer graphene narrow bands. *Phys. Rev. X* **8**, 031088 (2018).
16. Koshino, M. et al. Maximally localized Wannier orbitals and the extended Hubbard model for twisted bilayer graphene. *Phys. Rev. X* **8**, 031087 (2018).
17. Zou, L., Po, H. C., Vishwanath, A. & Senthil, T. Band structure of twisted bilayer graphene: Emergent symmetries, commensurate approximants, and Wannier obstructions. *Phys. Rev. B* **98**, 085435 (2018).
18. Xu, Y. et al. Correlated insulating states at fractional fillings of moiré superlattices. *Nature* **587**, 214–218 (2020).
19. Jin, C. et al. Stripe phases in WSe2/WS2 moiré superlattices. *Nat. Mater.* **20**, 940–944 (2021).
20. Regan, E. C. et al. Mott and generalized Wigner crystal states in wse2/ws2 moiré superlattices. *Nature* **579**, 359–363 (2020).
21. Morris, D. J. P. et al. Dirac strings and magnetic monopoles in the spin ice Dy2Ti2O7. *Science* **326**, 411–414 (2009).

22. Savary, L. & Balents, L. Quantum spin liquids: a review. *Rep. Prog. Phys.* **80**, 016502 (2016).
23. Kasteleyn, P. The statistics of dimers on a lattice: I. the number of dimer arrangements on a quadratic lattice. *Physica* **27**, 1209–1225 (1961).
24. Verberkmoes, A. & Nienhuis, B. Triangular trimers on the triangular lattice: an exact solution. *Phys. Rev. Lett.* **83**, 3986–3989 (1999).
25. Trambly de Laissardière, G., Mayou, D. & Magaud, L. Localization of Dirac electrons in rotated graphene bilayers. *Nano Lett.* **10**, 804–808 (2010).
26. Fang, S. & Kaxiras, E. Electronic structure theory of weakly interacting bilayers. *Phys. Rev. B* **93**, 235153 (2016).
27. Wong, D. et al. Local spectroscopy of moiré-induced electronic structure in gate-tunable twisted bilayer graphene. *Phys. Rev. B* **92**, 155409 (2015).
28. Li, G. et al. Observation of van hove singularities in twisted graphene layers. *Nat. Phys.* **6**, 109–113 (2010).
29. Po, H. C., Zou, L., Senthil, T. & Vishwanath, A. Faithful tight-binding models and fragile topology of magic-angle bilayer graphene. *Phys. Rev. B* **99**, 195455 (2019).
30. Villain, J. Commensurate-incommensurate transition of krypton monolayers on graphite: a low temperature theory. *Surf. Sci.* **97**, 219–242 (1980).
31. Coppersmith, S. N., Fisher, D. S., Halperin, B. I., Lee, P. A. & Brinkman, W. F. Dislocations and the commensurate-incommensurate transition in two dimensions. *Phys. Rev. B* **25**, 349–363 (1982).
32. Kang, J. & Vafek, O. Strong coupling phases of partially filled twisted bilayer graphene narrow bands. *Phys. Rev. Lett.* **122**, 246401 (2019).
33. Liang, R., Bonn, D. A. & Hardy, W. N. Evaluation of CuO_2 plane hole doping in $YBa_2Cu_3O_{6+x}$ single crystals. *Phys. Rev. B* **73**, 180505 (2006).
34. Rozen, A. et al. Entropic evidence for a Pomeranchuk effect in magic-angle graphene. *Nature* **592**, 214–219 (2021).
35. Xie, Y. et al. Fractional Chern insulators in magic-angle twisted bilayer graphene. *Nature* **600**, 439–443 (2021).
36. Zhang, S., Lu, X. & Liu, J. Correlated insulators, density wave states, and their nonlinear optical response in magic-angle twisted bilayer graphene. *Phys. Rev. Lett.* **128**, 247402 (2022).
37. Mao, D., Zhang, K. & Kim, E.-A. Work in preparation.

Acknowledgements

Author contributions
E.-A.K. and L.F. conceived the idea and supervised the project. K.Z. performed the theoretical analysis. Y.Z. carried out Monte Carlo analysis. All authors contributed to interpreting the results and writing the manuscript.

Competing interests
The authors declare no competing interests.

Additional information
Supplementary information The online version contains supplementary material available at https://doi.org/10.1038/s42005-022-01027-6.

Correspondence and requests for materials should be addressed to Kevin Zhang.

Peer review information *Communications Physics* thanks the anonymous reviewers for their contribution to the peer review of this work.

Reprints and permission information is available at http://www.nature.com/reprints

Publisher's note Springer Nature remains neutral with regard to jurisdictional claims in published maps and institutional affiliations.